Electronic Supplementary Material

Regulation of pseudographitic carbon domain to boost sodium energy storage

Zhidong Hou, Mingwei Jiang, Da Lei, Xiang Zhang, Yuyang Gao, and Jian-Gan Wang (✉)

State Key Laboratory of Solidification Processing, Center for Nano Energy Materials, School of Materials Science and Engineering, Northwestern Polytechnical University and Shaanxi Joint Lab of Graphene (NPU), Xi'an 710072, China

Supporting information to https://doi.org/10.1007/s12274-024-6448-1

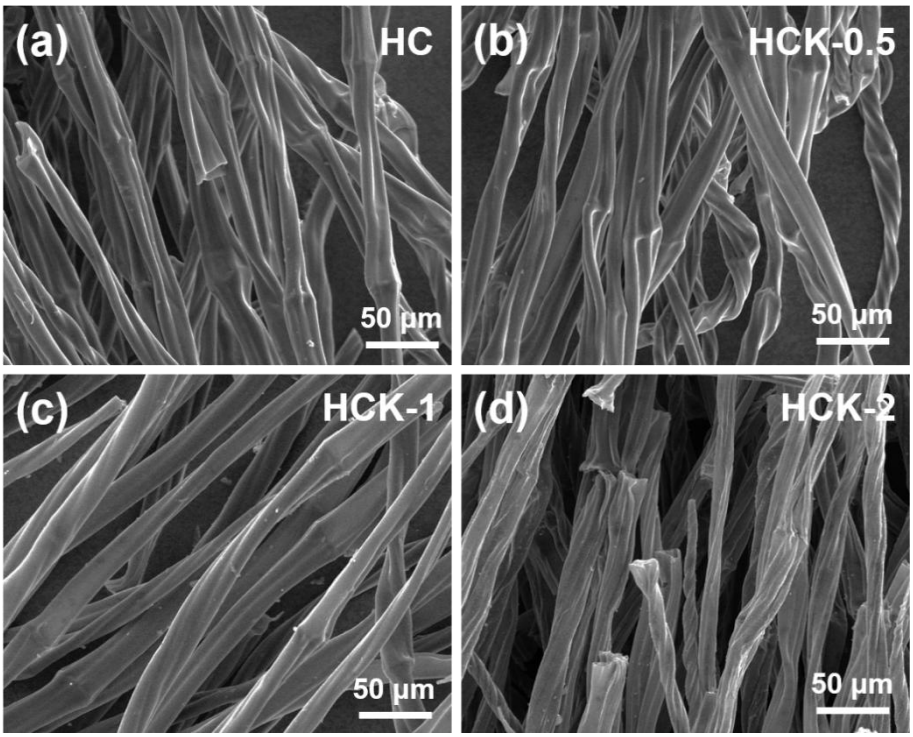

Figure S1 SEM images of (a) HC, (b) HCK-0.5, (c) HCK-1, and (d) HCK-2.

Address correspondence to wangjiangan@nwpu.edu.cn

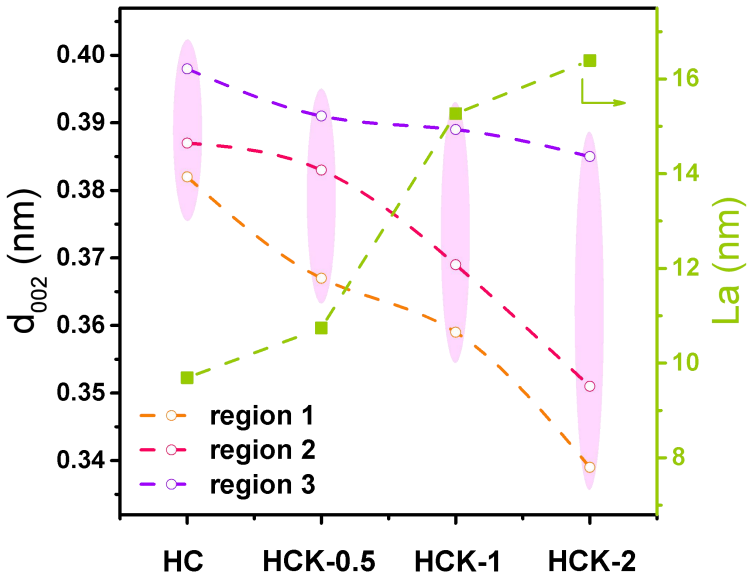

Figure S2 The d_{002} and La of hard carbon from TEM and Raman results.

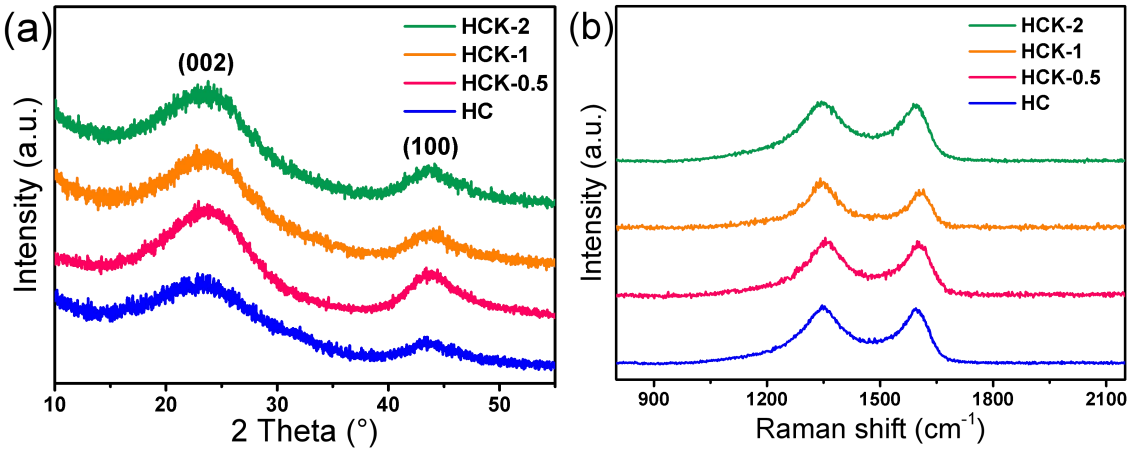

Figure S3 (a) XRD patterns and (b) Raman spectra of hard carbon materials.

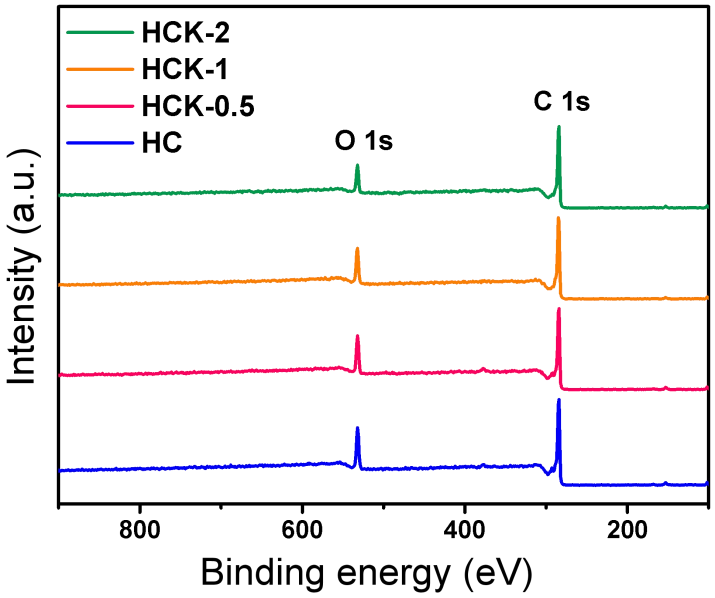

Figure S4 XPS full spectra of several hard carbon samples.

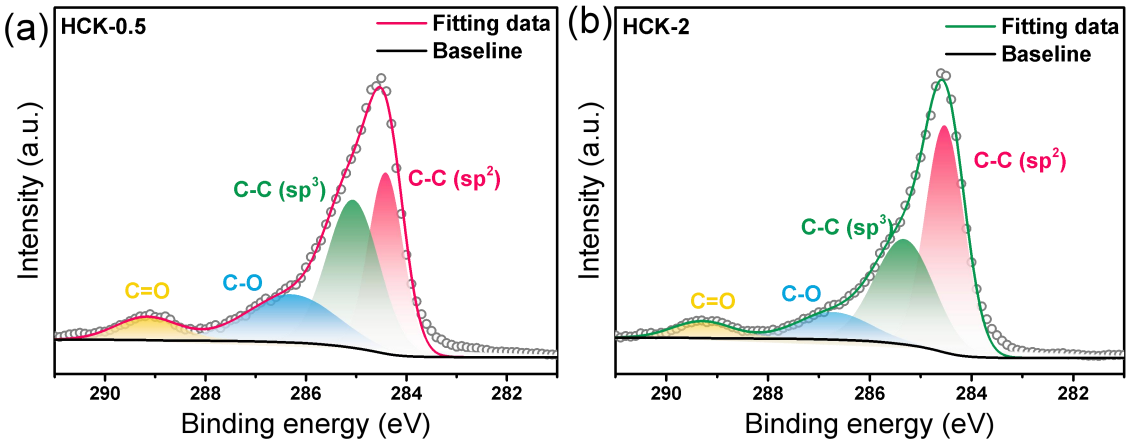

Figure S5 XPS C1s high resolution spectra of (a) HCK-0.5 and (b) HCK-2.

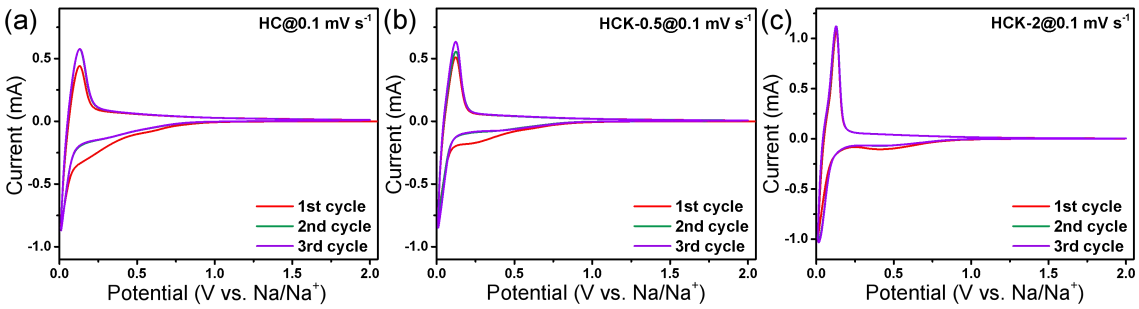

Figure S6 The CV curves of (a) HC, (b) HCK-0.5, and (c) HCK-2 electrodes at 0.1 mV s^{-1}.

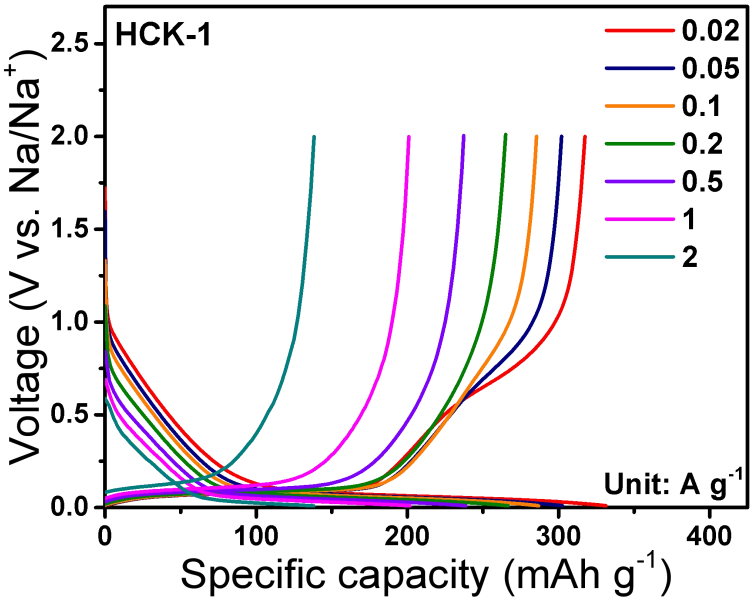

Figure S7 The discharge and charge profiles of the HCK-1 electrode at different current densities.

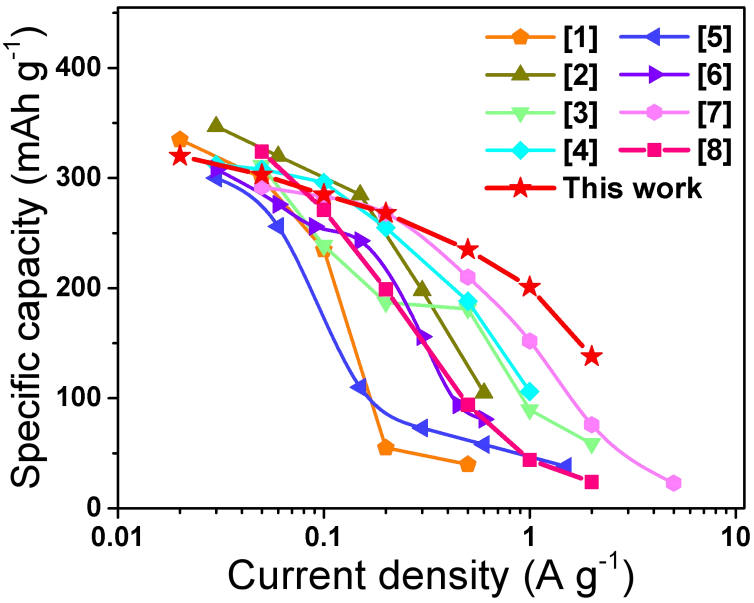

Figure S8 The Na storage performance comparison of the HCK-1 with other hard carbons from recent literatures.

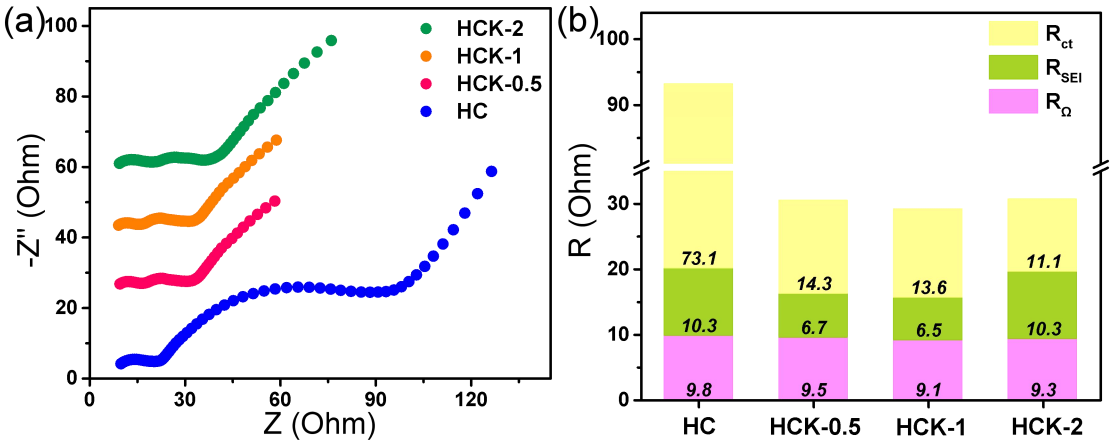

Figure S9 (a) The EIS plots and (b) R_{Ω}, R_{SEI}, and R_{ct} of different cycled electrodes.

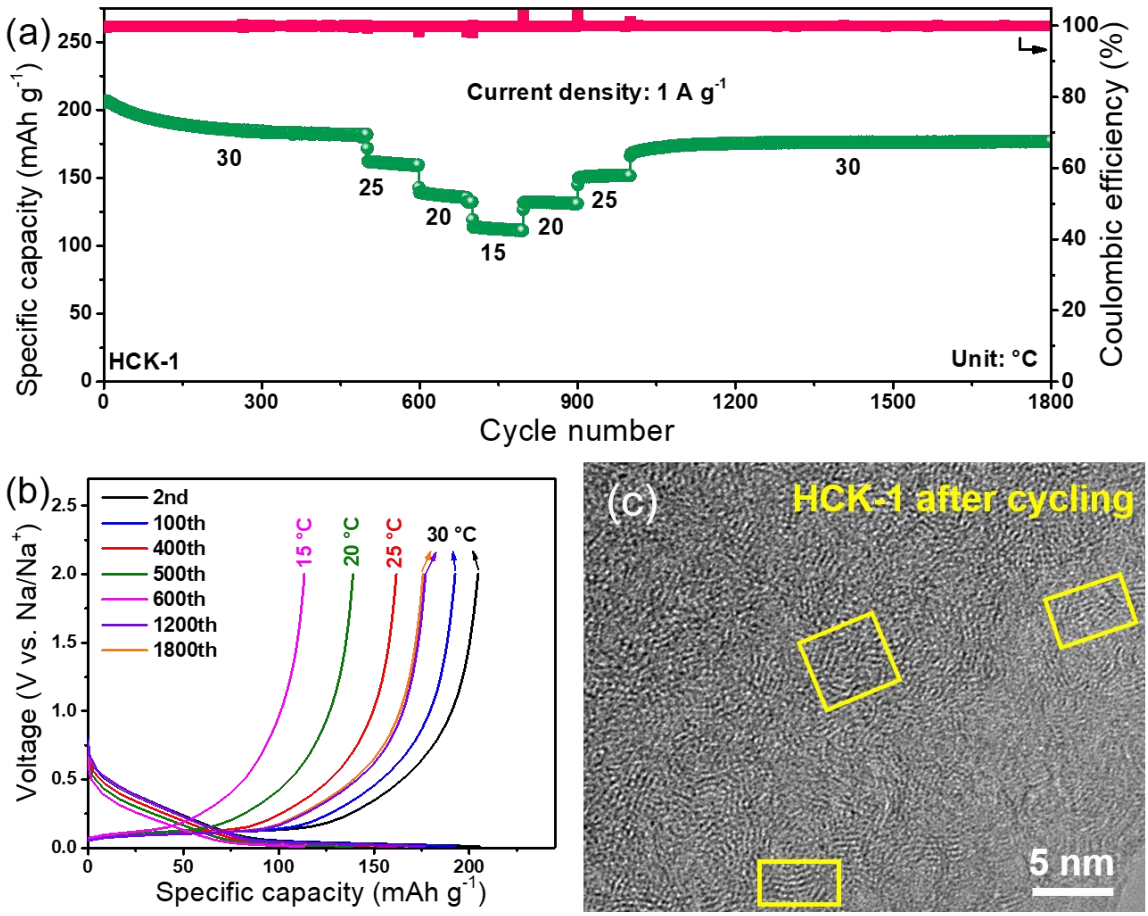

Figure S10 (a) Long-term cycling performance, (b) Galvanostatic discharge-charge profiles at 1 A g^{-1}, and (c) TEM image after cycling of HCK-1.

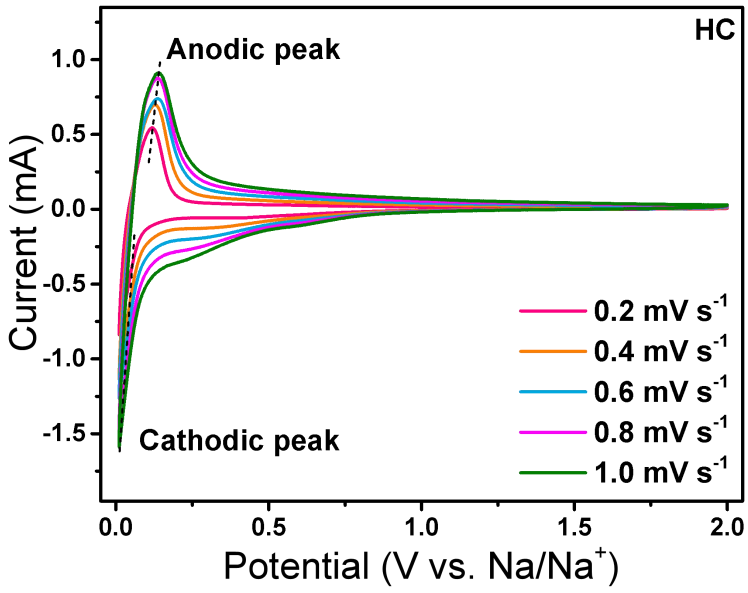

Figure S11 CV curves of HC at different rates.

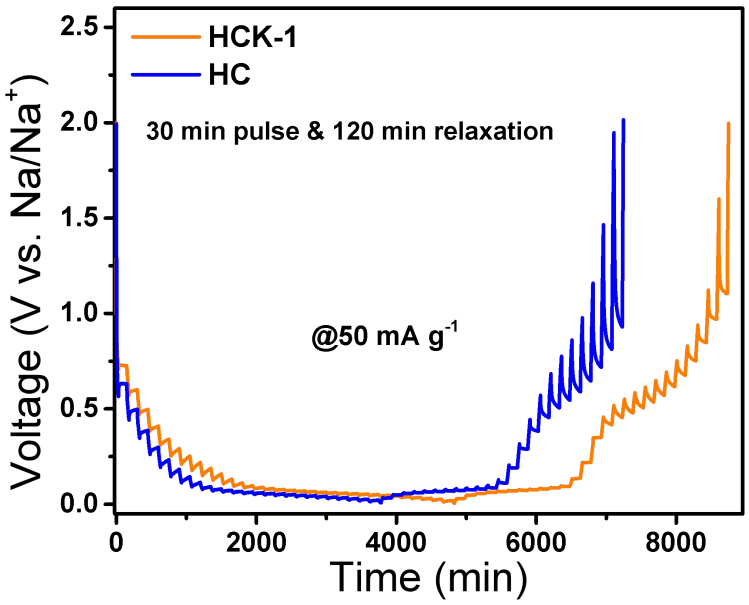

Figure S12 Voltage responses of HC and HCK-1 during the charging/discharging process.

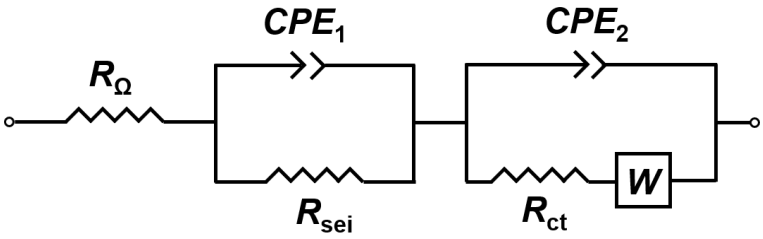

Figure S13 The equivalent circuit diagram for hard carbon electrodes: R_{Ω}, R_{sei}, R_{ct}, CPE, and W represent the internal resistance of cells, the SEI layer resistance, the charge transfer resistance, the constant phase element, and the Warburg resistance, respectively.

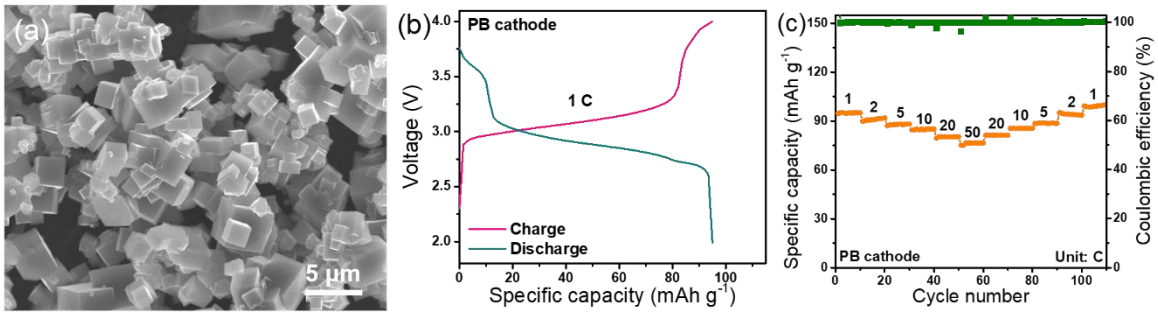

Figure S14 (a) SEM image of PB. (b) Galvanostatic discharge/charge curve and (c) rate property of PB cathode.

Table S1 The distribution proportion of high-resolution C1s species

Sample	C-C (sp^2)	C-C (sp^3)	C-O	C=O
HC	31.5%	45.9%	13.9%	8.8%
HCK-0.5	31.8%	39.1%	21.8%	7.3%
HCK-1	43.8%	37.7%	12.8%	5.7%
HCK-2	48.9%	34.6%	10.9%	5.5%

Table S2 The ICE of HC, HCK-0.5, HCK-1, and HCK-2 at 0.1 A g^{-1}

Sample	HC	HCK-0.5	HCK-1	HCK-2
Charge capacity (mAh g^{-1})	245.4	235.1	286.3	272.6
Disharge capacity (mAh g^{-1})	319.3	304.5	356.2	350.9
ICE (%)	76.9	77.2	80.4	77.7

Table S3 Comparison of electrochemical performance with different carbonaceous anodes materials reported

Ref.	Precursors	Treatment strategy	Na storage capacity (mAh g^{-1}) at 0.02/0.05/0.1/0.2/0.5/1/2 A g^{-1}
[1]	Paper towels	Catalytic defect-repairing	335/300/235/55/40/–/–
[2]	Glucose	Hydrothermal carbonization	347/320/285/198/105/–/–
[3]	Sugarcane	Microwave activation	–/311.3/238.7/187/89.5/58.7/–
[4]	Lignite coal	Cross-linking reaction	312/308/296/255/188.2/106.1/–
[5]	Polymer	Functional group engineering	300/256/110/73/58/–/38
[6]	Anthracite	Chemical pre-activation	308/276/256/243/156/81/–
[7]	Lignin	Closed pore construction	–/266/236/175/104/77
[8]	Tamarind fruit shell	Interlayer spacing expansion	–/324/271/199/94/44/24
This work	Platanus flosses	Molten-salt catalysis	320/303/285/268/235/201/138

Table S4 The fitted results of R_Ω, R_{sei}, and R_{ct} of HCK-1 during the first two cycles

Voltage	First cycle (Ω)			Second cycle (Ω)		
	R_Ω	R_{sei}	R_{ct}	R_Ω	R_{sei}	R_{ct}
OCV	7.8	-	30.4	7.6	1.3	1.0
1.5 V	7.7	-	29.7	8.3	1.0	1.3
1.0 V	7.9	-	20.8	7.6	1.6	1.6
0.7 V	7.9	-	20.0	7.5	1.3	1.4
0.4 V	8.0	-	16.8	7.8	1.8	3.9

0.1 V	8.2	-	15.9	8.2	2.1	3.9
0.05 V	8.2	-	12.5	8.4	4.9	3.6
0.01 V	8.1	-	9.2	8.3	3.6	4.3
0.05 V	8.3	7.3	3.6	7.8	1.7	4.5
0.1 V	7.9	2.3	4.5	7.4	1.7	1.6
0.4 V	7.5	2.3	2.0	7.4	1.6	1.1
0.7 V	7.5	2.1	1.1	7.1	1.4	1.3
1.0 V	7.4	2.1	1.0	7.3	1.2	1.2
1.5 V	7.5	1.3	1.0	7.4	1.0	1.1

References

[1] Zhao, J.; He, X. X.; Lai, W. H.; Yang, Z.; Liu, X. H.; Li, L.; Qiao, Y.; Xiao, Y.; Li, L.; Wu, X.; Chou, S. L. Catalytic defect‐repairing using manganese ions for hard carbon anode with high‐capacity and high‐initial‐coulombic‐efficiency in sodium‐ion batteries. *Adv. Energy Mater.* **2023**, *13*, 2300444.

[2] Xu, Z.; Wang, J.; Guo, Z.; Xie, F.; Liu, H.; Yadegari, H.; Tebyetekerwa, M.; Ryan, M. P.; Hu, Y. S.; Titirici, M. M. The role of hydrothermal carbonization in sustainable sodium‐ion battery anodes. *Adv. Energy Mater.* **2022**, *12*, 2200208.

[3] Yu, K.; Wang, X.; Yang, H.; Bai, Y.; Wu, C. Insight to defects regulation on sugarcane waste-derived hard carbon anode for sodium-ion batteries. *J. Energy Chem.* **2021**, *55*, 499-508.

[4] Chen, H.; Sun, N.; Wang, Y.; Soomro, R. A.; Xu, B. One stone two birds: Pitch assisted microcrystalline regulation and defect engineering in coal-based carbon anodes for sodium-ion batteries. *Energy Stor. Mater.* **2023**, *56*, 532-541.

[5] Tang, X.; Xie, F.; Lu, Y.; Chen, Z.; Li, X.; Li, H.; Huang, X.; Chen, L.; Pan, Y.; Hu, Y.-S. Intrinsic effects of precursor functional groups on the Na storage performance in carbon anodes. *Nano Research* **2023**.

[6] Wang, K.; Sun, F.; Wang, H.; Wu, D.; Chao, Y.; Gao, J.; Zhao, G. Altering thermal transformation pathway to create closed pores in coal‐derived hard carbon and boosting of Na^+ plateau storage for high‐performance sodium‐ion battery and sodium‐ion capacitor. *Adv. Funct. Mater.* **2022**, *32*, 2203725.

[7] Meng, Q.; Chen, B.; Jian, W.; Zhang, X.; Sun, S.; Wang, T.; Zhang, W. Hard carbon anodes for sodium-ion batteries: Dependence of the microstructure and performance on the molecular structure of lignin. *J. Power Sources* **2023**, *581*, 233475.

[8] Yu, K.; Zhao, H.; Wang, X.; Zhang, M.; Dong, R.; Li, Y.; Bai, Y.; Xu, H.; Wu, C. Hyperaccumulation route to Ca-rich hard carbon materials with cation self-incorporation and interlayer spacing optimization for high-performance sodium-ion batteries. *ACS Appl. Mater. Interfaces* **2020**, *12*, 10544-10553.